Fusion Engineering and Design 151 (2020) 111383

Contents lists available at ScienceDirect

Fusion Engineering and Design

journal homepage: www.elsevier.com/locate/fusengdes

Modeling of time-dependent gas pumping networks in the whole range of the Knudsen number: Simulation of the ITER dwell phase

Nikos Vasileiadis*, Dimitris Valougeorgis

Department of Mechanical Engineering, University of Thessaly, Pedion Areos, 38334, Volos, Greece

ARTICLE INFO

Keywords:
Kinetic modeling
Hybrid modeling
Vacuum gas dynamics
Vacuum systems
Gas distribution systems
ITER divertor

ABSTRACT

A hybrid time-dependent algorithm to simulate the transient response of gas distribution systems of arbitrary size and complexity, in the whole range of the Knudsen number, is proposed. The pressure evolution in the vessels is described by a simple macro model derived via mass conservation principals, while the pressure and mass flow rates in the pipe network are described by a micro model, consisting of the in-house steady-state gas network code "ARIADNE", based on kinetic theory. The two models are explicitly coupled, i.e. at each time step the gas network is solved via ARIADNE and the computed node pressures and pipe flow rates are provided to the macroscale evolution equations to update the vessel pressures. The proposed methodology and code are successfully validated by solving two prototype problems and comparing the results with corresponding ones available in the literature or obtained by Molflow+. The computational effectiveness and efficiency of the proposed approach to model large size networks is demonstrated by simulating the transient response of the ITER torus primary pumping system in the dwell phase. Interesting findings for the torus effective pumping speed and pressure evolution, including the final pressure at the end of the dwell phase are provided.

1. Introduction

Large gas pumping systems operating in a wide range of the Knudsen number play a significant role in fusion reactors [1,2] and particle accelerators [3]. In addition, vacuum gas distribution systems may be found in many industrial processes and technological fields including semiconductor technologies, material deposition, vacuum metallurgy, food packaging and metrology [4,5]. Since these systems operate from very low pressures ($\sim 10^{-10}$ Pa) up to atmospheric pressure, the gas flow may be from the free molecular regime up to the transition or even the slip and viscous flow regimes. To accurately simulate gas flows in a wide range of vacuum conditions, mesoscale kinetic modeling, as described by the Boltzmann equation or reliable kinetic model equations, is required [6]. However, in gas distribution networks with hundreds or thousands of piping elements, as the ones in large fusion reactors (e.g. in ITER), applying directly stochastic or deterministic kinetic modeling requires formidable computational resources and therefore, several alternative approaches have been developed.

The so-called electric-hydraulic analogy is frequently used in the free molecular and viscous limits [7,8]. In this classical approach, the gas distribution system is replaced by an equivalent electric circuit, where current and voltage correspond to gas flow rate and pressure respectively. Then, the steady-state or the transient response of the equivalent electric circuit may be simulated by typical integrated circuit codes. However, this methodology is valid only when the whole gas pipe network operates either in the free molecular or the viscous regimes.

Another more general approach has been elaborated in the ITERVAC code, developed at the Institute of Technical Physics in the Karlsruhe Institute of Technology [9,10]. Interpolating between available solutions in the free molecular and viscous regimes reliable semi-empirical expressions to compute the conductance through various pipe elements have been derived and implemented in ITERVAC to model gas pumping systems operating under various vacuum conditions. ITERVAC has been successfully applied to simulate several vacuum gas distribution systems including the ITER divertor pumping system [11]. The code is subject however, to steady-state conditions, as well as to certain theoretical simplifications.

Recently, an approach for simulating nanofluidic networks of long and narrow channels via a hybrid molecular-continuum method is presented in [12], based on the multiscale method proposed in [13,14]. Computational savings are primarily achieved by exploiting length-scale separation. Hybrid approaches are promising and must be investigated in multiscale physics problems. Of course, the distinction between the regions of the domain with different length scales (flow

* Corresponding author.
E-mail address: nikovasi@mie.uth.gr (N. Vasileiadis).

https://doi.org/10.1016/j.fusengdes.2019.111383
Received 29 July 2019; Received in revised form 18 October 2019; Accepted 26 October 2019

regimes) in order to apply the associated theory is not always a straightforward task.

In this framework, at the University of Thessaly (UTH) in Volos, Greece, an in-house code has been developed for simulating steady-state gas pumping distribution systems of arbitrary size and complexity in the whole range of the Knudsen number (free molecular, transition and viscous regimes) [15–17]. This is achieved by integrating a dense kinetic database providing the flow rates through pipe elements of various geometries subject to any pressure difference into a typical gas network solver. The flow rates are computed via kinetic modeling and they are very accurate since they are based on theoretical principles. The effectiveness of the developed UTH network code to model large size networks has been demonstrated in [17], where it has been successfully implemented to simulate various steady-state gas pumping scenarios of the ITER divertor system, providing results in good qualitative and quantitative agreement with corresponding ones based on alternative approaches, such as the ITERVAC code and the Direct Simulation Monte Carlo (DSMC) method [11,18]. It is noted that the UTH code has been developed within the European fusion program in an effort to simulate the vacuum pumping systems of tokamak type fusion reactors.

Furthermore, in several occasions the temporal response of the gas distribution pumping system is needed. This is readily seen in gas pumping scenarios, where the input operational data are varying with time or the pressure of the vacuum system must be reduced to a certain threshold value. A specific application of such flow setup is the dwell phase operation of fusion reactors (e.g. ITER), where the torus vacuum vessel must be evacuated between consecutive plasma shots. Although, this specific application plays a significant role in the efficiency of fusion machines it has not been thoroughly investigated in the literature [19,20]. In general, as far as the authors are aware of, the transient response of large size gas distribution systems has not been studied in a systematic manner. In the present work the in-house UTH steady-state network code is upgraded and accordingly implemented to simulate time-dependent gas distribution systems subject to transient boundary conditions. In the present work the time-dependent behavior of the whole pipe network is achieved in a hybrid manner [21]. At each time step, the steady-state flow configuration is solved, based on kinetic modeling, to compute the amount of gas pumped out from each vacuum vessel through the pipe network and then, the pressure of all vacuum vessels is updated by applying the mass conservation principle and the equation of state.

The next sections of the paper are structured as follows: In Section 2, the components and input data of a typical gas distribution network are provided (Section 2.1), the steady-state part of the algorithm, focusing on certain advancements performed in the present work, is described (Section 2.2) and the proposed hybrid time-dependent algorithm is presented (Section 2.3). In Section 3, the proposed transient methodology and algorithm are validated in two benchmark flow configurations. The first one is related to gas expansion into vacuum and the second one to a distribution system with two vacuum vessels and one pump. The temporal evolution of the pressures are compared in the former case with DSMC results available in the literature [22,23] and in the latter case with results obtained by the Test particle Monte Carlo (TPMC) code Molflow+ [24]. In Section 4, the transient dwell phase pump-down of the ITER fusion reactor is simulated and the obtained results include the torus effective pumping speed with respect to the torus pressure, as well as, the temporal evolution of the torus pressure. Concluding remarks are presented in Section 5.

2. Formulation of the time-dependent algorithm

2.1. Definition of gas distribution system components and algorithm input data

The components of a typical gas distribution system and the associated input data in the gas network algorithm are provided.

In general, a gas distribution system may be modeled by a pipe network represented by an undirected graph consisting of n nodes and p piping elements acting as the connections between two nodes [25]. A variety of node types may be used to represent the different components of a gas pipe network. More specifically, junctions between two or more pipes are represented by the inner nodes n_i, vessels and pumps are represented by the vessel nodes n_v and pump nodes n_p respectively, while constant pressure regions are represented by the so-called fixed-pressure nodes n_f. The total number of nodes is $n = n_i + n_f + n_v + n_p$. Furthermore, closed paths formed by connecting adjacent nodes and open paths formed by connecting two fixed-pressure, vessel or pump nodes are named loops and pseudoloops respectively. Both of them are involved in the formulation of the equations modeling the network. The number of independent loops and pseudoloops, in a well-defined network, are given by $l = p - n + 1$ and $l_p = (n_f + n_v + n_p) - 1$ respectively. The loops and pseudoloops of the network are determined by the well-known depth-first-search algorithm (DFS) [26]. The DFS algorithm is a graph traversing procedure which starts at an arbitrary node and explores the graph as far as possible before backtracking.

A schematic representation of a sample network for demonstration and clarity purposes is shown in Fig. 1. It consists of $n = 9$ nodes and $p = 10$ pipes. The total number of nodes includes $n_i = 6$ inner nodes (circles), $n_f = 1$ fixed-pressure nodes (squares), $n_v = 1$ vessel node (pentagon) and $n_p = 1$ pump node (triangle). Also, there is a set of $l = 2$ independent loops and $l_p = 2$ pseudoloops denoted by l_1, l_2 and pl_1, pl_2 respectively.

To complete the description of the network configuration, additional geometrical data are needed. It is very important to properly specify the node ($i = 1, ...,n$) and pipe ($j = 1, ...,p$) indexing, the type of each node and the connectivity matrix defining the connections between the nodes of the network. Also, the length L_j and the hydraulic radius $R_{h,j}$ for each piping element $j = 1, ...,p$, as well as the volume V of the vessel at each vessel node are specified. It is noted that unless otherwise stated, all piping elements are considered as circular tubes and the hydraulic radius concept is applied in the case of non-circular piping elements.

Next, the operational input data of the gas distribution system are provided. They commonly include the molar mass and the viscosity of the pumped gas species, the network temperature T, the constant pressure values P_i at the fixed pressure nodes, the initial pressure $P_i(t_0)$ at the vessel nodes at some initial time t_0, the flow demand (gain or loss) W_i at the inner nodes, the outgassing or gas injection data $Q_{in,i}(t)$ at all vessel nodes and the characteristic pumping speed - inlet pressure curve $S_i^*(P_i)$ of all pumps. In the case of no flow demand or outgassing or gas injection the corresponding quantities are set equal to zero. In the sample network of Fig. 1 some of the required operational data are

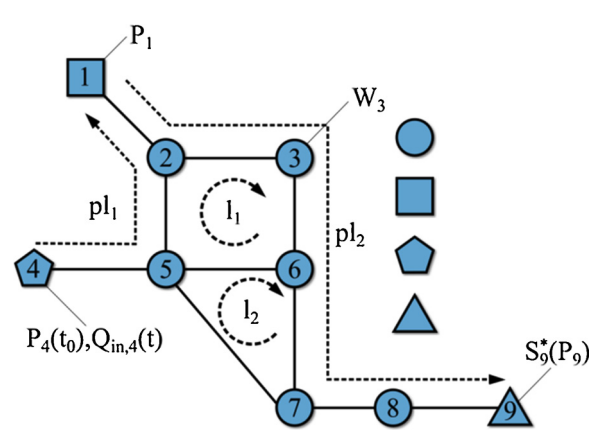

Fig. 1. Schematic representation of a sample network with indicative geometrical and operational data.

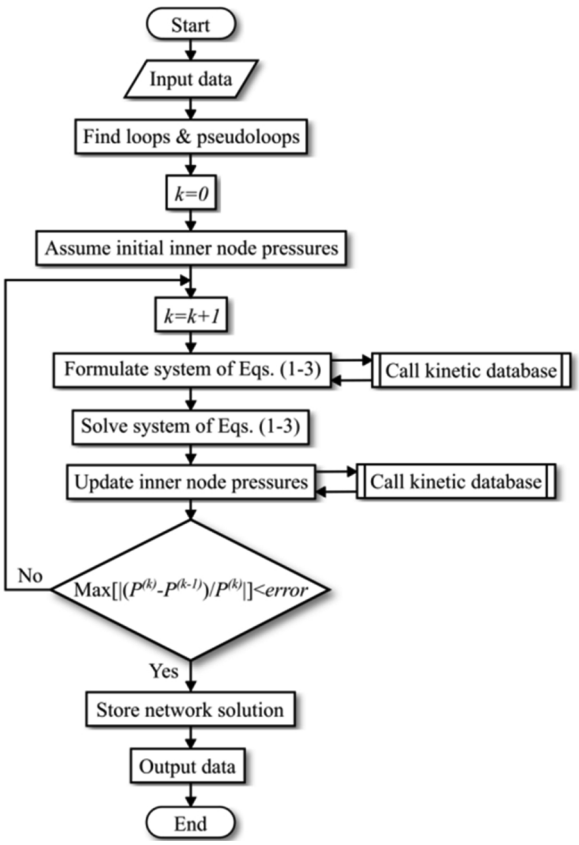

Fig. 2. Flowchart of the UTH steady-state code applied in [17].

shown for demonstration purposes. At fixed-pressure node 1 the pressure is P_1, at inner node 3 the flow demand is W_3, at vessel node 4 the initial pressure is $P_4(t_0)$ and the outgassing data are given by some $Q_{in,4}(t)$ and at the pump node 9 the characteristic curve is defined as $S_9^*(P_9)$.

All above described geometrical and operational data must be provided in the algorithm in order to advance in the simulation of the steady-state or the transient response of the gas distribution network.

2.2. The upgraded UTH steady-state network code

The algorithm of the UTH steady-state network code is first briefly reviewed mainly for completeness and clarity purposes. The flowchart of this code is shown in Fig. 2. Then, certain code advancements, which are performed in the present work and are integrated in the steady-state code, required for its extension to the transient model, are also presented. The flowchart of the upgraded UTH steady-state network code is shown in Fig. 3.

Starting with the brief review of the code, shown in the flowchart of Fig. 2, it is seen that the solution of the pipe network is obtained in an iterative manner assuming initially the pressure at all inner nodes. In each iteration, the following linear algebraic system, consisting of the mass conservation equations at the inner nodes

$$\sum_j (\pm \dot{M}_{i,j}) - W_i = 0, \qquad i = 1, \ldots, n_i \tag{1}$$

and the energy conservation equations along the loops

$$\sum_j (\pm \Delta P_{k,j}(\dot{M}_{k,j})) = 0, \qquad k = 1, \ldots, l \tag{2}$$

and pseudoloops

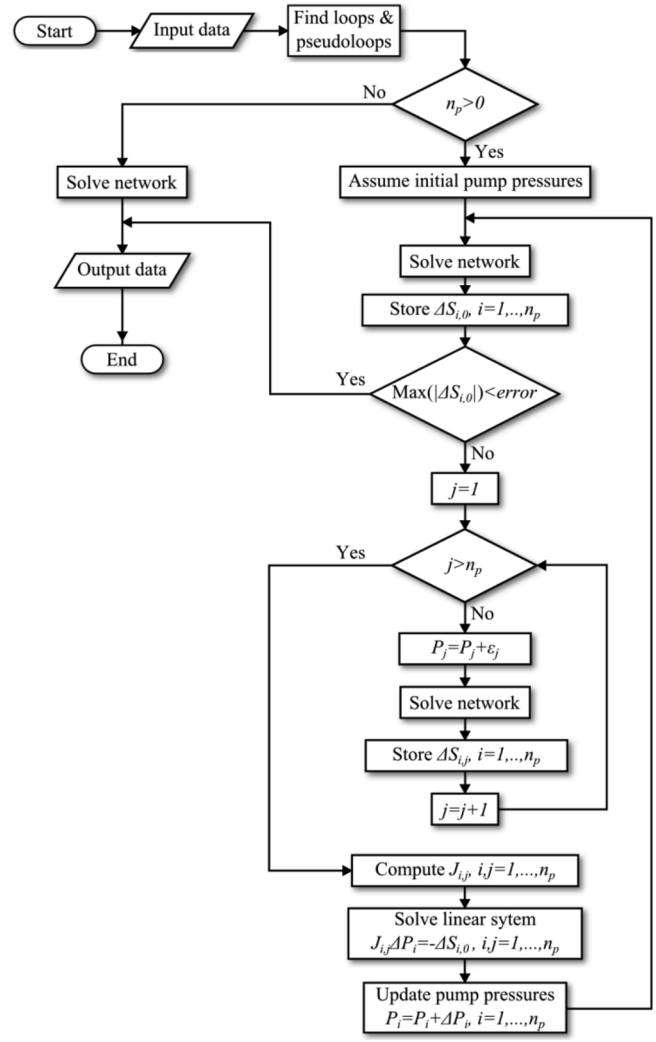

Fig. 3. Flowchart of the present upgraded UTH steady-state code (ARIADNE).

$$\sum_j (\pm \Delta P_{m,j}(\dot{M}_{m,j})) = \Delta P_m, \qquad m = 1, \ldots, l_p \tag{3}$$

is solved. The summation index j refers, in Eq. (1) to the pipes connected to node i and in Eqs. (2) and (3) to the pipes included in loop k and pseudoloop m respectively. In Eq. (1), the unknown quantities $\pm \dot{M}_{i,j}$ are the mass flow rates at node i from pipe j. The plus and minus signs correspond to flow into and out of the node respectively. Also, the quantities $\pm W_i$ denote the known mass flow demand at some node i and they are taken as positive or negative when they are exiting or entering the system respectively. In Eqs. (2) and (3), the quantities $\pm \Delta P_{k,j}$ and $\pm \Delta P_{m,j}$ are the pressure difference between the inlet and outlet pressure of pipe j and depend on the respective mass flow rates $\dot{M}_{k,j}$ and $\dot{M}_{m,j}$. The plus sign is used if the flow in pipe j is in the clockwise direction or otherwise the minus sign is employed. In Eq. (3), ΔP_m is the pressure difference between the first and the last pseudoloop nodes. Depending on the specific geometrical and operational data for each pipe element, the pressure differences in the energy balance equations (2) and (3) are substituted by kinetic theory expressions in terms of the associated mass flow rates deducing a closed system of algebraic equations to be solved for the unknown mass flow rates. It is noted that the dimensionless flow rates involved in the aforementioned kinetic expressions are obtained by a micro model that consists of the kinetic solution of pressure-driven flows through pipes in the whole range of the involved parameters. A detailed description of the involved kinetic expressions is provided in [17].

Once the linear system is solved and the mass flow rates of all piping elements are computed, all inner node pressures are updated based on the kinetic pressure drop relations and are compared to the previous ones. The iterative procedure is continued until the relative pressure difference between two successive iterations at all inner nodes is smaller than a specified value.

In addition to the inner node pressures and the pipe mass flow rates, the network solution also provides the pipe conductance

$$C_i = \frac{\dot{M}_i}{(\Delta P)_i} R_g T_0, \quad i = 1, \ldots, p \tag{4}$$

and the pumping speed of the pump

$$S_i = \frac{Q_i}{P_i} = \frac{\dot{M}_i R_g T_0}{P_i}, \quad i = 1, \ldots, n_p \tag{5}$$

where T_0 is a reference temperature, $R_g = k_B/m$ is the specific gas constant (k_B is the Boltzmann constant and m the molar mass) and Q_i denotes the pump throughput or the so-called PV flow. Both the conductance and the pumping speed are of major practical interest in vacuum gas dynamics.

Continuing with the upgraded UTH steady-state code, shown in the flowchart of Fig. 3, it is noted that the main advancement refers to pipe networks with a single or multiple pumps. In this case an additional iterative procedure is required, in order to meet the pumping speed restrictions, i.e. to satisfy the pumping speed - inlet pressure $S_i^*(P_i)$ at each pump node. Following the initial assumption of the pump pressures, the network solver, as described above (Fig. 2), is applied to compute the pipe mass flow rates and the node pressures of the network, including the pumping speeds at the pump nodes. The pumping speed differences between the obtained solution $S_{i,0}(P_{i,0})$ and the given pumping speed curve $S_i^*(P_i)$, defined as $\Delta S_{i,0} = (S_i^*(P_{i,0}) - S_{i,0}(P_{i,0}))/S_i^*(P_{i,0})$, is computed and stored for all pumps $i = 1, \ldots, n_p$.

Next, all pump pressures are set to the initial pressure assumption except for a specific pump pressure P_j, which is changed by a small amount ε_j. The network is solved again and the pumping speed differences $\Delta S_{i,j} = (S_i^*(P_{i,j}) - S_{i,j}(P_{i,j}))/S_i^*(P_{i,j})$ are computed and stored for all pump nodes $i = 1, \ldots, n_p$. This computation is performed for all pumps $j = 1, \ldots, n_p$ and when it is completed, the Jacobian $J_{i,j} = (\Delta S_{i,j} - \Delta S_{i,0})/\varepsilon_i$, $i, j = 1, \ldots, n_p$ is constructed.

Then, the linear system of equations $J_{i,j} \times \Delta P_i = -\Delta S_{i,0}$ is solved and all pump pressures are updated as $P_i = P_i + \Delta P_i$. The procedure is repeated until the network solution with regard to the pumping speeds fulfills the convergence criterion imposed on $\Delta S_{i,0}$. The applied methodology is Newton's iterative method, where the partial derivatives are numerically computed and its convergence close to the solution is superlinear.

It is important to note that in the aforementioned iterative method, the main computational effort is due to the initial network solution to compute $\Delta S_{i,0}$. The subsequent solutions of the network for each pump $j = 1, \ldots, n_p$ in order to compute $\Delta S_{i,j}$ converge much faster than the initial one (generally in a single iteration) and this is achieved by taking the inner node pressures of the previous network solution as the initial assumption of the inner node pressures for the current network solution. Thus, the involved computational effort is only slightly increased by increasing the number of pumps in the network.

In addition to the above, the involved kinetic data bases, needed in the implementation of the steady-state network code, have been accordingly enriched with more dense flow rate results in terms of the operating conditions and geometrical data. Also, efficient interpolating algorithms have been integrated in the code to improve its accuracy. The steady-state code has been restructured based on object-oriented programming to facilitate its accessibility, adaptation and implementation in various technological applications.

All these advancements significantly increase the robustness and the efficiency of the steady-state network code. It is noted that the hybrid time-dependent simulation of the gas distribution system, described in the next subsection, involves the solution of a steady-state network configuration in each time step.

In order to facilitate the discussion in the rest of the paper, as well as for future reference, an acronym is given to the upgraded UTH steady-state code. The acronym is "**ARIADNE**" and stands for **A**lgorithm for **R**arefied gas flow in **A**rbitrary **D**istribution **Ne**tworks.

2.3. The hybrid time-dependent algorithm

Algorithms coupling computational techniques at different scales are defined as hybrid algorithms. The direct simulation of time-dependent gas pumping scenarios can be computationally very expensive, even in comparatively small or moderate size vacuum systems. Particularly, in large size vacuum systems, such as the ITER divertor pumping system, the computational cost of a direct time-dependent approach is prohibitive. In cases where a time scale separation is applicable the hybrid time-dependent approach proposed in [21], explicitly coupling a macro model for the vessels of the gas distribution system with a micro model for the piping elements, may be implemented to significantly reduce computational effort.

The time characterizing the flow inside the piping elements is defined as the time needed to cross a characteristic length with the most probable molecular speed $\upsilon_0 = \sqrt{2R_g T}$ of the conveying gas and is given by

$$t_m = R_h/\upsilon_0 \tag{6}$$

where R_h is the hydraulic radius of the piping element, R_g is the specific gas constant and T is the network temperature. The corresponding characteristic time inside a vessel is [21]

$$t_M = V/(\upsilon_0 R_h^2) \tag{7}$$

where V is the volume of the vessel.

Since the macroscopic quantities in the vessels vary in a much slower pace than those in the pipes it is readily seen that $t_M >> t_m$ (e.g. the instantaneous variation of the mass flow rate in the piping elements modifies the vessel pressure in a quasi-steady manner). Therefore, it is reasonable to exploit the time scale separation and investigate separately the network vessels and pipes by the corresponding macro and micro models, which are explicitly coupled in sequence (not simultaneously). The micro model is consisting of the upgraded UTH steady-state code (ARIADNE) described in the previous subsection.

The macro model describing the temporal evolution of pressure $P_i(t)$ in some vacuum vessel i can be derived by considering the mass balance in the vessel and the equation of state. It is easily deduced that

$$V_i \frac{dP_i(t)}{dt} = Q_{in,i}(t) + \dot{M}_i(t) R_g T \tag{8}$$

where the throughput $Q_{in,i}(t)$ is entering the vacuum vessel at some time t due to either outgassing or direct gas injection inside the vacuum vessel and the mass flow rate $\dot{M}_i(t)$ is entering (positive) or exiting (negative) the vacuum vessel through the piping elements connecting the vessel with the distribution system (pipe network). Equation (8) can also be written in terms of the effective vessel pumping speed $S_{eff,i}(t)$ in the equivalent form

$$V_i \frac{dP_i(t)}{dt} = Q_{in,i}(t) - P_i(t) S_{eff,i}(t). \tag{9}$$

It is noted that, in the notation used $S_{eff,i}(t)$ is considered as positive when gas is pumped out of the vessel i. The ordinary differential equations (8) or (9), defining the macro model, subject to the corresponding initial conditions $P_i(t_0)$, are numerically solved by typical integration schemes (e.g. Runge Kutta methods) once the macroscale time integration step Δt is specified.

The coupling between the macro and micro models is rather simple and it is shown in the flowchart of Fig. 4. At each macroscale time step

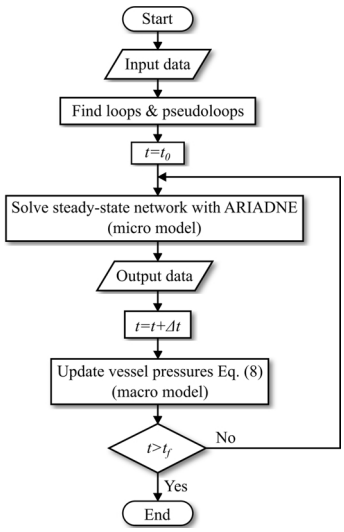

Fig. 4. Flowchart of the hybrid time-dependent algorithm.

the gas distribution system is solved via ARIADNE, which includes a micro model computing the dimensionless flow rates at each pipe of the network in the whole range of the Knudsen number. Thus, at some certain time t, based on the current input conditions, the mass flow rates and the pressures of the network are computed. The output data are written to respective output files. The time is updated as $t + \Delta t$, the vessel node pressures are updated via Eq. (8) or (9) (macro model) and the algorithm can move to the next time step. The evolution in time proceeds until a specified final time t_f or an equilibrium state is reached.

The computational gain of the hybrid time-dependent algorithm is due to the fact that ARIADNE is only implemented at each macroscale and not microscale time step. The proposed time-dependent algorithm is benchmarked in the next section.

3. Benchmarking of the time-dependent algorithm

The time-dependent algorithm implementing the ARIADNE code at each time step is validated by solving two prototype problems.

The first prototype problem involves gas expansion into vacuum. More specifically, the dynamic standard apparatus for the measurement of the response and relaxation times of vacuum gauges developed by Physikalische-Technische Bundesanstalt (PTB) is considered [22]. In Fig. 5, the schematic representation of the flow setup of prototype problem 1 is provided. Two vessels, namely the upstream and downstream vessels with volumes $V_1 = 3.1$ l and $V_2 = 185$ l respectively, are interconnected via a circular tube with length $L = 0.492$ mm and radius $R_h = 0.50565$ mm. The valve between the two vessels is closed. The upstream vessel is filled with a monatomic gas up to an initial pressure of $P_1(t_0 = 0) = 1000$ Pa, while the downstream vessel is evacuated via a turbomolecular pump to a negligible pressure. Next, the valve rapidly opens and time-dependent gas expansion between the two vessels occurs. The turbomolecular pump keeps running during the whole

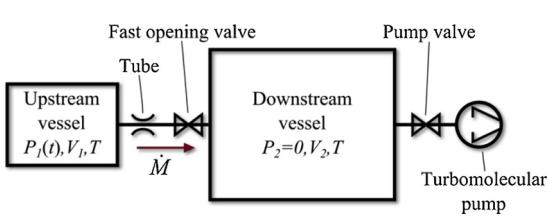

Fig. 5. Schematic representation of the gas expansion network (prototype problem 1).

Table 1
Gas properties of He, Ne, Ar and Kr.

Gas	He	Ne	Ar	Kr
Molar mass [Kg/Kmol]	4.003	20.18	39.95	83.80
Viscosity at 295 K [μPas]	19.70	30.89	22.80	24.86

experiment in order to maintain high vacuum at the downstream vessel ($P_2 = 0$ Pa). This flow setup has been considered in [23] and the temporal evolution of the upstream pressure vessel $P_1(t)$ for the monatomic gases of He, Ne, Ar and Kr has been obtained both computationally and experimentally indicating very good comparison between the corresponding results. The computational work in [23] is based on the same hybrid scheme implemented in the present work, with the steady-state solution at each time step however obtained by the DSMC method.

In the ARIADNE code the above configuration is represented as a vessel node (upstream vessel) connected with a fixed-pressure node (downstream vessel) via a single piping element. The input data include the vessel volume V_1, the length L and radius R_h of the tube, the initial upstream pressure $P_1(t_0 = 0)$, the fixed-pressure $P_2 = 0$ Pa and the time-step $\Delta t = 10^{-4}$ s. Also, the conveying gas properties, shown in Table 1, are provided.

In Fig. 6 the temporal evolution of the upstream vessel pressure $P_1(t)$ computed by the present time-dependent algorithm is plotted for all four monatomic gases. The experimental and computational results in [23] are also provided for comparison purposes. As it is clearly seen there is always an excellent agreement between the corresponding results. It is noted that the agreement between the present computational results and the experimental results of [23] is improved compared to the corresponding one reported in [23] and this is mainly contributed to the more dense kinetic database and interpolation algorithms implemented in ARIADNE. Based on this comparison, the proper implementation of the hybrid time-dependent scheme in the ARIADNE code is demonstrated.

The second prototype problem involves the transient response of a small size pipe network in the free molecular regime and its comparison with the well-established TPMC code Molflow+ [24]. In Fig. 7, the schematic representation of the network of prototype problem 2 is provided. It consists of two vacuum vessels, with volumes $V_1 = V_2 = 8$ l, one cryogenic pump, with sticking coefficient 0.8, running at all times and five piping elements. The nodes 1 and 2 are vessel nodes, the nodes 3, 4 and 5 are inner nodes and node 6 is a pump node. A sample

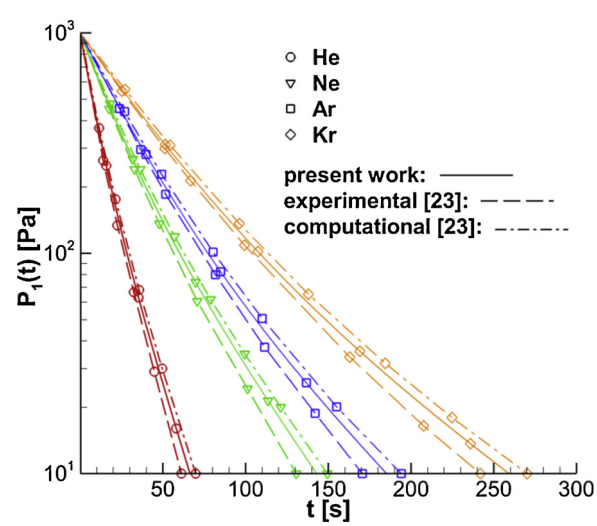

Fig. 6. Temporal evolution of the upstream vessel pressure for He, Ne, Ar and Kr in prototype problem 1; comparison between the present time-dependent algorithm and [23].

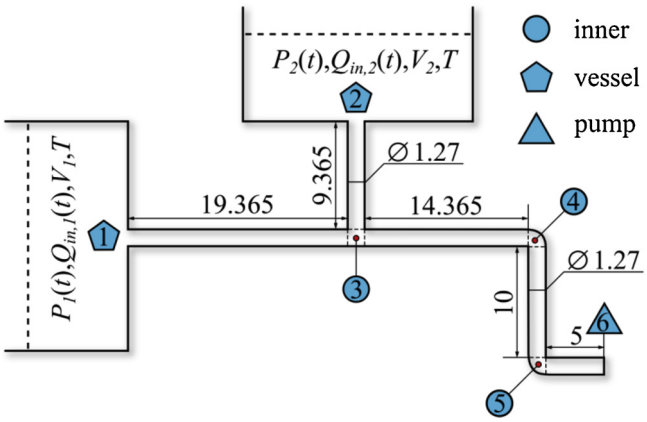

Fig. 7. Schematic representation of the pipe network in the free molecular regime (prototype problem 2).

material inside vessel V_1 is outgassing helium at a rate of $Q_1(t) = 2.5 \times 10^{-3} e^{-2t}$ Pam^3/s, while $Q_2(t) = 0$ Pam^3/s. The length and the radius of the pipes are given in Fig. 7. On purpose, the ratios of the length over the radius are in a wide range, varying from 7.87 up to 30.5, in order to have a more complete comparison.

In the TPMC time-dependent simulation the above network has been designed in the open source software Salome [27] and has been imported into Molflow+, along with all input data. The network has been simulated for 10 s by Molflow+ and the computed temporal pressure evolution at the six network nodes $i = 1, ..., 6$, is shown in Fig. 8. In addition, from the Molflow+ simulation the pumping speed at the pump node is found to be constant throughout the simulation and equal to 4.8 m^3/s. This constant pumping speed value (instead of the sticking coefficient) has been imported as input data in the ARIADNE code, since the pumping speed - inlet pressure curve must be defined for all pumps. Having properly defined all input data, the present time-dependent algorithm is implemented. The deduced temporal pressure evolution at the six nodes of the network, are also plotted in Fig. 8. In all cases an excellent agreement between corresponding results is observed, with the average relative deviation at each node ranging from 0.7% up to 4.4%. The smallest and largest deviations correspond to nodes 1 (outgassing vessel) and 5 (the elbow before the pump).

From the qualitative point of view the reported transient response of the system is well expected. At vessel node 1, the pressure P_1, is initially

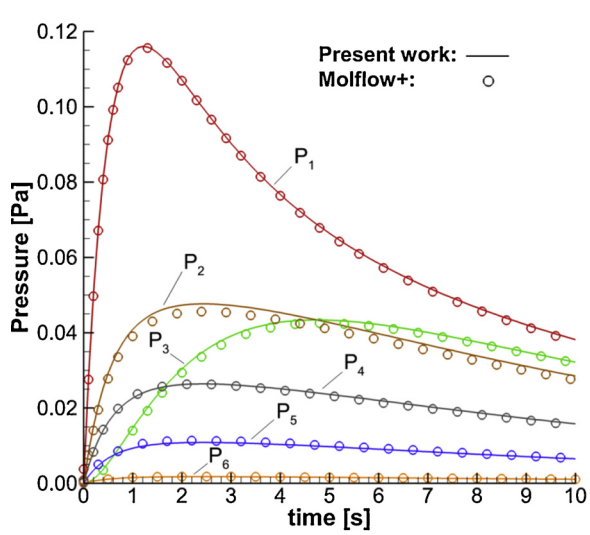

Fig. 8. Temporal evolution of pressure $P_i(t)$ at the six nodes $i = 1, ..., 6$ of prototype problem 2; comparison between the present time-dependent algorithm and Molflow+.

increased due to the high outgassing rates at small times up to some maximum value and then, as the outgassing is decreased, the pressure is monotonically decreased due to the presence of the continuously running pump. At inner nodes 2–5 the pressure evolution follows a similar trend, obtaining however smaller maximum values. At pump node 6, the pressure always remains very close to zero.

Based on the solution of these two prototype problems, the implementation of the proposed hybrid scheme is validated and the accuracy of the obtained results is confirmed, to some extend. Having developed some confidence on the proposed time-dependent algorithm, its effectiveness in modeling large size networks is demonstrated by simulating, in the next section, the time-dependent dwell phase of ITER.

4. The transient response of the ITER divertor system in the dwell phase

4.1. Geometrical and operational data including outgassing

The latest design of the ITER divertor consists of 54 cassettes with a 20 mm gap between adjacent cassettes and six direct cryopumps located at lower ports 4, 6, 10, 12, 16, 18 [2]. The configuration of the pipe network approximating the ITER divertor pumping system has been thoroughly described in [17] and therefore only a brief review is provided here for completeness and clarity purposes. The only difference between the aforementioned network configuration and the one implemented in the present work is a small modification in the pumping ducts concerning neutron shielding [28].

In Fig. 9, the cross section of a cassette connected to a cryogenic pump along with the pipe network approximating the actual gas flow in the cassette is shown. Each of the 54 cassettes has been approximated by a pipe network consisting of 43 nodes and 43 pipes. Nodes 1 to 26 and 27 to 43 correspond to the so-called upper and lower cassette parts respectively, which are connected via two pipes connecting nodes 1–27 and 9-33. In addition, in Fig. 9 the pumping duct network consisting of 7 nodes (not numbered) and 7 pipes, used to approximate the gas flow from a divertor cassette towards a direct cryopump is presented.

In Fig. 10, the pipe network approximating the 20 mm gap between two adjacent cassettes, consisting of 15 nodes and 41 pipes, is shown. It is seen that the gap network allows the gas to flow between adjacent cassettes through the toroidal connections located at nodes 6, 9, 15, 17, 21, 28, 31, 33, 35, 38 and 48. The gap pipe network also allows the gas to circulate inside the 20 mm gap.

Totally, the resulting pipe network for the ITER divertor gas system, modeling the torus primary pumping system, consists of $54 \times (43 + 15) + 6 \times 7 = 3174$ nodes and $54 \times (43 + 41) + 6 \times 7 = 4578$ pipes. All the reported results refer to the network configuration described above.

Continuing with the operational data the so-called "Inductive I" operation mode of ITER consists of 400 s burn and 1400 s dwell phases. During the dwell phase the ITER vacuum vessel, having a volume of 1400 m^3, must be pumped down to the threshold pressure of 5×10^{-4} Pa in order to start the next plasma shot [19]. The main impediment to the torus evacuation is the outgassing of hydrogen isotopes and helium implanted on the vacuum vessel walls during the plasma discharge.

Obviously, the outgassing data of the ITER torus during the dwell-phase are of major importance for the time-dependent simulations and are obtained following [19], where a realistic estimation of the ITER outgassing rate is given by considering corresponding data from JET. The outgassing rate from the beryllium wall of JET follows an inverse power law, written as [29]

$$Q_{in}(t) = K_1 t^{-n} \tag{10}$$

where K_1 is the initial outgassing rate, t is the dwell phase elapsed time and n is the decay index. Substituting Eq. (10) into Eq. (8) and (9) yields the macro model describing the temporal evolution of the ITER torus pressure $P(t)$ as

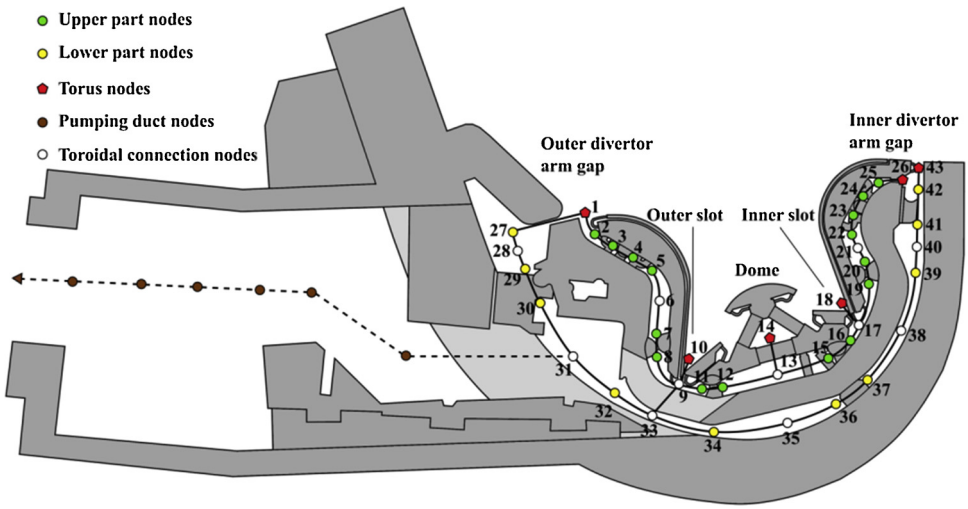

Fig. 9. Cross section view of a cassette connected to a pump along with the pipe network approximating the actual gas flow path.

$$V\frac{dP(t)}{dt} = K_1 t^{-n} + \dot{M}(t)R_g T = K_1 t^{-n} - P(t)S_{eff}(t) \tag{11}$$

where V is the volume of the torus and $S_{eff}(t)$ the torus effective pumping speed. For constant effective pumping speed at the torus, Eq. (11) is trivially solved analytically to deduce the closed form expression

$$P(t) = \left(P(t_0)e^{\frac{S_{eff}}{V}t_0} + \frac{K_1}{V}\int_{t_0}^{t} x^{-n}e^{\frac{S_{eff}}{V}x}dx\right)e^{-\frac{S_{eff}}{V}t} \tag{12}$$

where $P(t_0)$ is some known initial pressure at time t_0. The analytical solution (12), subject to the assumption of constant pumping speed, will be implemented in Section 4.2 for comparing and physically justifying some of the results.

It is noted that Eqs. (10–12) hold for $t > 0$ and thus, following [12], the dwell phase is assumed to start at $t = 1$ s, where by setting $dP/dt = 0$, according to Eq. (11), results to $Q_{in}(1) = K_1 = P(1)S_{eff}(1)$. Based on the experimental data from six consecutive JET pulses #70530 - #70535 [30] and the JET torus effective pumping speed of $S_{eff,JET} \sim 200\,\mathrm{m^3/s}$, the initial outgassing rate of the vacuum vessel is estimated between $1.2 - 1.5\,\mathrm{Pam^3/s}$. Thus, assuming the active vessel areas of JET and ITER being $144\,\mathrm{m^2}$ [31] and $700\,\mathrm{m^2}$ respectively [19], the initial outgassing rate of the ITER vessel is estimated between $5.8 - 7.2\,\mathrm{Pam^3/s}$. The decay index n has been repeatedly reported in the literature to range between $0.65 - 0.85$ [29,31,32].

Three pumping scenarios are investigated. In the first one the 2 pumps located at lower ports 4 and 6 are operating and the remaining 4 pumps are regenerating, while in the second one the 4 pumps located at lower ports 4, 6, 10 and 12 are running and the remaining 2 pumps are regenerating. It is noted that the chosen 2 and 4 pump port configuration corresponds to the worst case scenario i.e the minimum torus effective pumping speed of all possible port configurations. In the third pumping scenario all 6 cryopumps are operating. The latter scenario has been investigated for completeness purposes, although in practice all 6 pumps will not be used at the same time. The limiting pumping speed of the cryopumps is considered to be $55\,\mathrm{m^3/s}$ at the reference temperature of 273.15 K. Since the ITER torus and divertor system temperature may vary, the temperatures of 400, 600 and 800 K are considered. The conveying gas is D_2 (molar mass 4.028 Kg/Kmol,

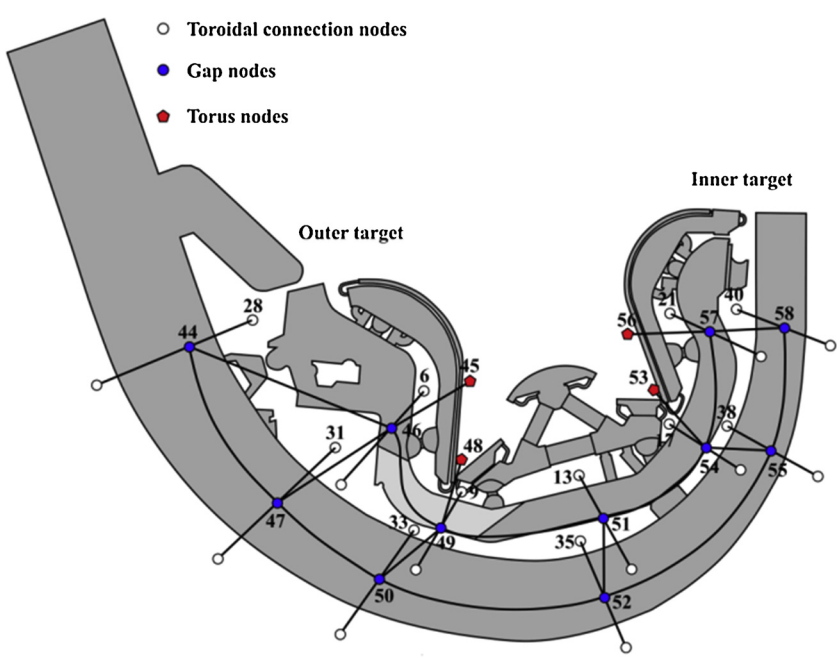

Fig. 10. Cross section view of a gap between adjacent cassettes along with the pipe network approximating the actual gas flow path.

Table 2
Torus effective pumping speed (m^3/s) of D_2 for various torus pressures with 2, 4 and 6 pumps running at 400, 600 and 800 K.

Pumping scenario	2 pumps			4 pumps			6 pumps		
Torus pressure [Pa]	400 K	600 K	800 K	400 K	600 K	800 K	400 K	600 K	800 K
10^{-5}	39.16	50.20	59.63	77.22	98.94	117.5	114.2	146.3	173.6
10^{-4}	39.17	50.21	59.64	77.25	98.95	117.5	114.3	146.3	173.6
10^{-3}	39.28	50.30	59.71	77.46	99.12	117.6	114.5	146.5	173.8
10^{-2}	40.33	51.18	60.48	79.47	100.8	119.1	117.2	148.7	175.7
10^{-1}	48.61	58.58	67.16	95.01	114.8	131.7	138.4	167.7	192.8
1	79.10	96.07	107.0	152.6	184.0	204.6	225.3	267.7	295.9

viscosity of 10.89, 14.34, 17.43 μPas at 400, 600 and 800 K) as the main outgassing hydrogen isotope [31].

4.2. Results and discussion

Before proceeding with the transient response of the ITER torus primary pumping system, some steady-state results of the ITER torus effective pumping speed in terms of the torus pressure are provided. The pressure at the torus pressure nodes (the pentagonal nodes in Figs. 9 and 10), is specified and it is introduced, along with the other needed geometrical and operational data into the ARIADNE code, which is implemented to find the mass flow rates and pressures in the divertor network, including the torus effective pumping speed.

In Table 2, tabulated rates of the torus effective pumping speed for torus node pressures equal to [10^{-5}, 10^{-4}, 10^{-3}, 10^{-2}, 10^{-1}, 1] Pa are provided based on the 2, 4 and 6 running pump scenarios at temperatures 400, 600 and 800 K. It is observed that when the torus node pressure is less than or equal to 10^{-3} Pa, i.e., when flow is in the free molecular regime, the torus pumping speed is almost constant and consequently the pumped throughput is linear with respect to pressure. On the contrary, when the torus node pressure is higher than $\sim 10^{-3}$ Pa, i.e., when the flow is in the transition regime, the torus pumping speed increases monotonically with the torus pressure. These remarks are valid for all three running pump scenarios. Furthermore, with the 4 and 6 pumps scenario the torus effective pumping speed is about 2 and 3 times higher than the corresponding one with the 2 pumps, respectively. This behavior indicates that, in both the 4 and 6 pumps scenarios the flow is not limited by the divertor and each cryopump added to the system, pumps about the same amount of gas as the other ones.

Turning next to the time-dependent problem, in Fig. 11, the temporal evolution of the ITER torus pressure during the 1400 s dwell phase, computed based on the present time-dependent algorithm, implementing the ARIADNE code at each time step, is compared with the corresponding one, based on the closed form expression (12) subject to the constant torus effective pumping speed assumption. The comparison is made for the three pumping scenarios at $T = 400$ K, with initial torus pressure equal to 1 Pa, average initial outgassing rate $K_1 = 6.5$ Pam^3/s and $n = 0.65$ and 0.85, which are the lower and upper limiting values of the decay index. Furthermore, the constant pumping speed in Eq. (12) is taken from Table 2 for torus pressure 10^{-5} Pa, equal to 39.16 m^3/s, 77.22 m^3/s and 114.2 m^3/s for the 2, 4 and 6 running pumps respectively. The specific values have been chosen since, based on the results of Table 2, the assumption of the constant pumping speed is justified in the low pressure regime.

As it is seen in Fig. 11, the results are in good qualitative agreement in the whole dwell phase. However, for $t \leq 300$ s, $t \leq 200$ s and $t \leq 100$ s in the cases of 2, 4 and 6 pumps respectively, there are significant quantitative deviations, with the present time-dependent algorithm considered as the accurate prediction. These discrepancies are justified, since for all above specified times the torus pressure is above 10^{-3}Pa (i.e the gas flow in the transition regime) and the torus effective

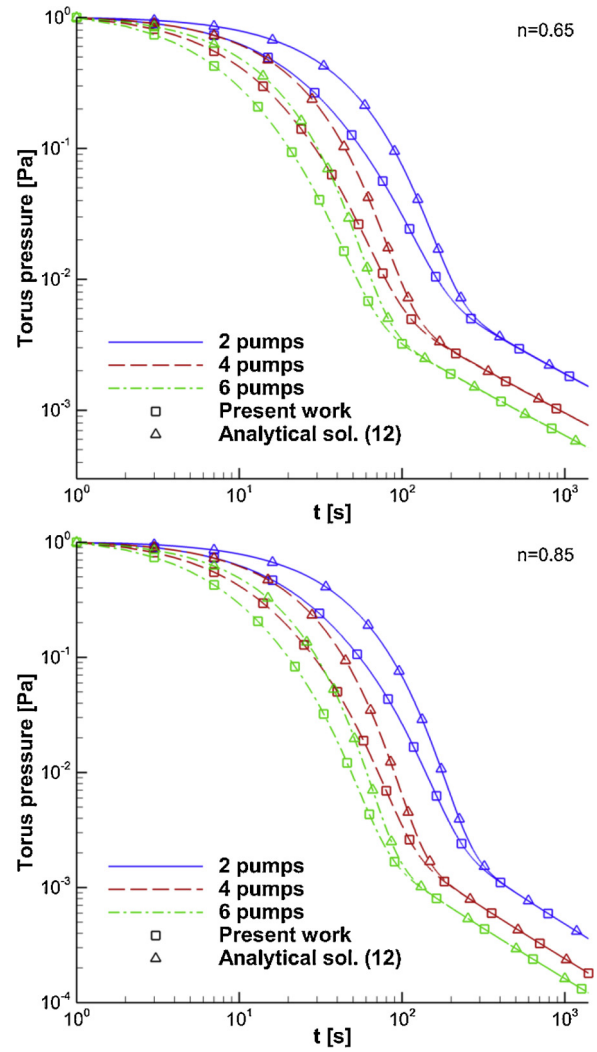

Fig. 11. Temporal evolution of the ITER torus pressure, based on ARIADNE and analytical solution (12), with 2, 4 and 6 pumps operating, initial torus pressure 1 Pa, initial outgassing rate $K_1 = 6.5$ Pam^3/s, temperature $T = 400$ K and decay indices $n = 0.65$ (up) and $n = 0.85$ (down).

pumping speed in all three pumping scenarios is not constant as clearly seen in Table 2, which makes the analytical solution of Eq. (12) invalid. On the contrary for $t > 300$ s, $t > 200$ s and $t > 100$ s in the cases of 2, 4 and 6 pumps respectively, with the torus pressure being below $\sim 10^{-3}$Pa and the whole pumping system in the free molecular regime the two approaches show excellent quantitative agreement. The observations with regard to the validity of the two approaches are important for the following reasons: a) The effectiveness of the present time-dependent algorithm in modeling the transient response of large size pipe networks is validated; b) When the torus pressure at the end of the 1400 s dwell phase is the only quantity of interest, it can be accurately predicted directly from Eq. (12), based on the constant torus pumping speed in the free molecular regime computed by ARIADNE, without implementing the hybrid time-dependent algorithm; c) The physical behavior of the torus pressure temporal evolution including the final torus pressure at the end of the 1400 s dwell phase can be qualitatively explained based on the simple form of Eq. (12). This third remark is employed later on in the discussion of the torus pressure evolution.

The temporal evolution of the torus pressure during the dwell phase for initial torus pressures equal to 1, 10^{-1} and 10^{-2} Pa is plotted in Fig. 12. The other data are as before (three pumping scenarios, $T = 400$ K, $K_1 = 6.5$ Pam^3/s, $n = 0.65$ and 0.85). Starting with the 2 pumps

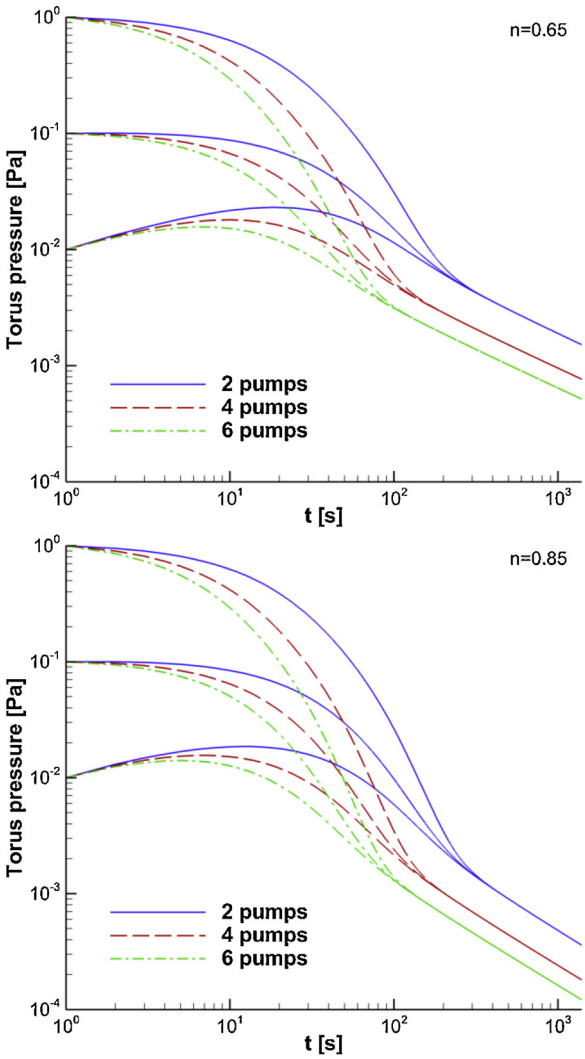

Fig. 12. Temporal evolution of the ITER torus pressure for initial torus pressures $P(1) = [10^{-2}, 10^{-1}, 1]$ Pa, with 2, 4 and 6 pumps operating, initial outgassing rate $K_1 = 6.5$ Pam^3/s, temperature $T = 400$ K and decay indices $n = 0.65$ (up) and $n = 0.85$ (down).

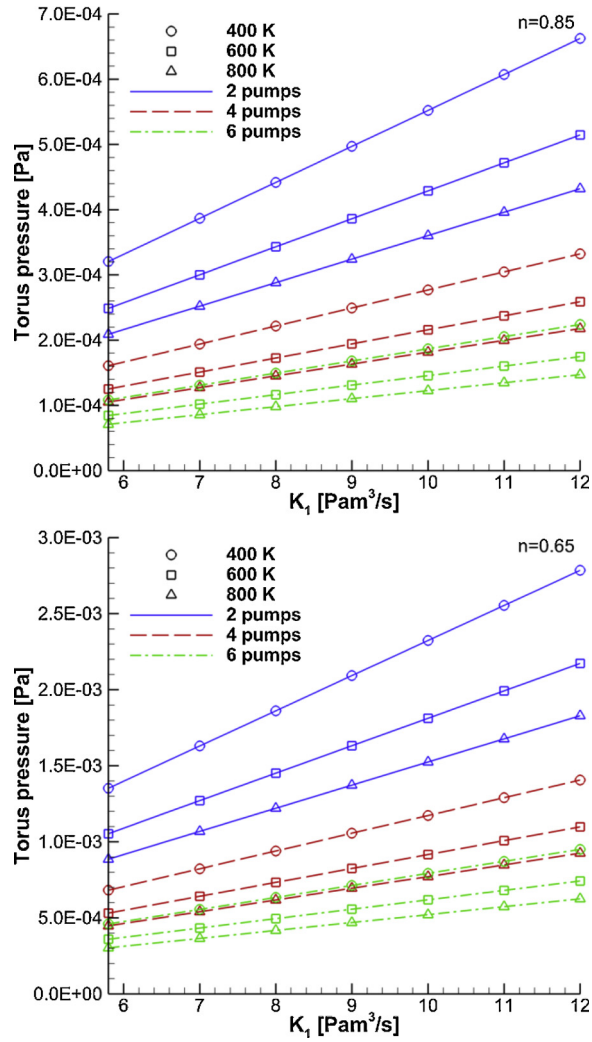

Fig. 13. Torus pressure after the 1400 s dwell phase in terms of the initial outgassing rate K_1 with 2, 4 and 6 pumps operating, temperature $T = 400$, 600 and 800 K and decay indices $n = 0.85$ (up) and $n = 0.65$ (down).

scenario, it is seen that the torus pressure evolution depends on the initial torus pressure when approximately $t \leq 300$ s, while it becomes identical for all initial pressure conditions when $t > 300$ s. The observed behavior also holds with the 4 or 6 pumps scenarios, with the corresponding times, where the merging of the torus pressure temporal evolution curves takes place, at approximately $t = 100$ s and $t = 200$ s respectively. These remarks are valid for both decay indices. Thus, it may be concluded that in the range of the investigated parameters the torus pressure after the 1400 s dwell phase period is independent from the initial pressure conditions of the torus. The above remark is easily justified by examining the right hand side of expression (12), where the first term, related to the initial pressure is constant, while the second term, related to outgassing, grows with time. Therefore, at adequately large times the temporal pressure evolution will be independent of the initial pressure conditions and will only depend on the outgassing term, assuming that K_1, $S_{eff} > 0$.

Since many of the required ITER dwell phase data have been either extrapolated from corresponding JET data or have been assumed, a parametric study is performed in order to deduce some useful information on the overall effectiveness of the pumping scenarios in ITER. In Fig. 13 the final torus pressure after the 1400 s dwell phase is presented in terms of the initial outgassing rates K_1 for the decay indices $n = 0.65$ and 0.85, the system temperatures $T = 400$, 600 and 800 K with the 2, 4 and 6 pumps operating.

It is readily seen that in all cases the final torus pressure grows linearly with the initial outgassing rate. This trend is justified by Eq. (12), where K_1 multiplies the growing with time outgassing term, which is the one, as mentioned above, affecting the final torus pressure. Furthermore, the final torus pressure with the 4 and 6 pumps scenarios is always reduced about 2 and 3 times respectively, compared to the corresponding one with the 2 pumps scenario. As mentioned above the torus effective pumping speed is increased by about 2 and 3 times when 4 and 6 cryopumps are employed. However, a robust connection between the linear dependence of the two effects, via Eq. (12), has not been established. It is also seen that the final torus pressure is reduced as the torus temperature is increased. More specifically, when the torus temperature is increased from 400 K to 600 K the final torus pressure is always decreased by about 22%, while when the torus temperature is doubled from 400 K to 800 K the torus pressure reduction is about 34%. In addition, for $n = 0.85$, corresponding to the lowest outgassing scenario, after the 1400 s dwell pumping the target torus pressure of 5×10^{-4} Pa can be always achieved in the cases of 4 and 6 running pumps, while in the case of 2 operating pumps it is achieved only in a certain range of the investigated parameters. For $n = 0.65$, corresponding to the highest outgassing scenario however, the required threshold pressure is marginally achieved in the expected range of

initial outgassing rates (5.8-7.2Pam^3/s) only when all 6 cryopumps are employed. Actually, even with the utilization of all 6 cryopumps, considering the uncertainty of the initial outgassing rate estimation (extrapolated from JET), it cannot be stated with absolute certainty, that the threshold pressure of 5×10^{-4} Pa can be achieved when $n = 0.65$.

Based on the presented results and the associated discussion, the feasibility and effectiveness of the proposed time-algorithm, implementing ARIADNE at each macroscale time step, in modeling the time response of large size gas distribution systems is demonstrated. In parallel some findings concerning the operation of the ITER torus primary pumping system in the dwell phase have been presented.

5. Concluding remarks

The in-house UTH code for simulating steady-state gas distribution systems of arbitrary size and complexity in rarefied conditions has been advanced to include the computation of the pumping speeds of the network pumps in a robust and automatic self-consistent manner. Also, an enriched, denser kinetic data base of the piping elements flow rates has been integrated into the network solver, to provide more accurate results in the whole range of the Knudsen number. The code has been restructured based on object-oriented programming to be more accessible to the user and easily implemented in large size networks. For future reference, the in-house upgraded UTH steady-state code is named "**ARIADNE**", standing for **A**lgorithm for **R**arefied gas flow in **A**rbitrary **D**istribution **Ne**tworks.

Furthermore, a time-dependent algorithm, based on an explicit hybrid scheme, is proposed, to simulate the transient response of gas distribution systems with varying operating conditions. The response time scale separation of the network vessels and piping elements is exploited and they are investigated separately by the corresponding macro and micro models, which are explicitly coupled. The macro model, describing the pressure evolution in the network vessels, consists of simple ordinary differential equations derived via mass conservation principles, while the micro model, describing the pressure and mass flow rate evolution in the pipe network, consists of the steady-state code ARIADNE. Coupling between the two models is achieved by solving at each macroscale time step the gas distribution system via the micro model and providing the flow rates to the macro model to compute the pressure in the vessels for the next time step. The computational gain is significant since ARIADNE is implemented only at each macroscale time step.

The presented code has been successfully benchmarked by solving two prototype problems and comparing the results with corresponding ones available in the literature, as well as with the well-established code Molflow+. In both cases excellent agreement has been observed.

Next, the effectiveness of the time-dependent algorithm to model large size networks is demonstrated by simulating the ITER time-dependent dwell phase with the duration of 1400 s for various operating scenarios. Several interesting findings are reported. Regarding the torus pressure at the end of the dwell phase, which is of major importance, it has been found that it is independent of the initial torus pressure conditions, it increases linearly with the initial outgassing rate and it decreases as the network temperature increases. It is also seen that the final torus pressure with the 4 and 6 pump scenario is reduced about 2 and 3 times compared to the corresponding one with the 2 pump scenario. Concerning the specified target pressure of 5×10^{-4} Pa at the end of the dwell phase, based on the present simulations subject to the introduced operational and geometrical data, it is concluded that in the lowest outgassing scenario it can be achieved in a wide range of the investigated parameters, while on the contrary in the highest outgassing scenario it is marginally achieved only in the expected range of initial outgassing rates when all 6 cryopumps are employed.

It is believed that the presented software has a lot of potential and of course it may be further advanced. Although both the steady-state (ARIADNE) and time-dependent hybrid algorithms have been developed within the EUROfusion program in an effort to simulate the pumping systems of tokamak type fusion reactors, they can be also applied in gas distribution systems of other technological fields.

Declaration of competing interest

The authors declare that they have no known competing financial interests or personal relationships that could have appeared to influence the work reported in this paper.

Acknowledgements

This work has been carried out within the framework of the EUROfusion Consortium and has received funding from the Euratom research and training programme 2014-2018 and 2019-2020 under grant agreement No 633053. The views and opinions expressed herein do not necessarily reflect those of the European Commission. Part of this work has been performed by using computational resources provided by the MARCONI-FUSION HPC.

References

[1] R.J.H. Pearce, A. Antipenkov, et al., Gas species, their evolution and segregation through the ITER vacuum systems, Vacuum 86 (2012) 1725–1730.
[2] R.J. Pearce, A. Antipenkov, B. Boussier, S. Bryan, M. Dremel, B. Levesy, C. Mayaux, M. Wykes, The ITER divertor pumping system, design evolution, simplification and performance, Fusion Eng. Des. 88 (2013) 809–813.
[3] J.M. Jimenez, LHC: The world's largest vacuum systems being operated at CERN, Vacuum 84 (2009) 2–7.
[4] K. Jousten (Ed.), Handbook of Vacuum Technology, Wiley-VCH Verlag GmbH & Co. KGaA, Weinheim, Germany, 2016.
[5] S. Naris, N. Vasileiadis, D. Valougeorgis, A.S. Hashad, W. Sabuga, Computation of the effective area and associated uncertainties of non-rotating piston gauges FPG and FRS, Metrologia 55 (2019) 015005.
[6] F. Sharipov, Rarefied Gas Dynamics: Fundamentals for Research and Practice, Wiley-VCH, 2016.
[7] W. Steckelmacher, Knudsen flow 75 years on: the current state of the art for flow of rarefied gases in tubes and systems, Rep. Prog. Phys. 49 (1986) 1083–1107.
[8] J.C. Schönfeld, Analogy of hydraulic, mechanical, acoustic and electric systems, Appl. Scientific Res. B 3 (1) (1954) 417–450.
[9] C. Day, V. Hauer, G. Class, D. Valougeorgis, M. Wykes, Development of a simulation code for ITER vacuum flows, IAEA Fusion Energy Conference (2006).
[10] C. Day, A. Antipenkov, M. Dremela, H. Haasa, V. Hauera, A. Macka, D.K. Murdoch, M. Wykes, R&D and design for the cryogenic and mechanical vacuum pumping systems of ITER, Vacuum 81 (2007) 738–747.
[11] V. Hauer, C. Day, ITER divertor gas flow modelling, Fusion Eng. Des. 98 (2015) 1775–1778.
[12] D. Stephenson, D.A. Lockerby, M.K. Borg, J.M. Reese, Multiscale simulation of nanofluidic networks of arbitrary complexity, Microfluid. Nanofluid. 18 (2015) 841–858.
[13] M.K. Borg, D.A. Lockerby, J.M. Reese, A hybrid molecular-continuum simulation method for incompressible flows in micro/nanofluidic networks, Microfluid. Nanofluid. 15 (2013) 541–557.
[14] M.K. Borg, D.A. Lockerby, J.M. Reese, A multiscale method for micro/nano flows of high aspect ratio, J. Comput. Phys. 233 (2012) 400–413.
[15] S. Misdanitis, D. Valougeorgis, Design of steady-state isothermal gas distribution systems consisting of long tubes in the whole range of the Knudsen number, J. Vac. Sci. Technol. 29 (2011) 061602.
[16] S. Misdanitis, D. Valougeorgis, Modeling of ITER related vacuum gas pumping distribution systems, Fusion Eng. Des. 88 (2013) 2352–2356.
[17] N. Vasileiadis, G. Tatsios, S. Misdanitis, D. Valougeorgis, Modeling of complex gas distribution systems operating under any vacuum conditions: Simulations of the ITER divertor pumping system, Fusion Eng. Des. 103 (2016) 125–135.
[18] C. Gleason-González, S. Varoutis, V. Hauer, C. Day, Simulation of neutral gas flow in a tokamak divertor using the direct simulation Monte Carlo method, Fusion Eng. Des. 89 (2014) 1042–1047.
[19] M. Wykes, P. Andrew, C. Day, G. Federici, Assessment of the ITER dwell pump-down, 21st IEEE/NPS Symposium on Fusion Engineering (2005).
[20] K. Battes, C. Day, V. Rohde, Basic considerations on the pump-down time in the dwell phase of a pulsed fusion DEMO, Fusion Eng. Des. 100 (2015) 431–435.
[21] M. Vargas, S. Naris, D. Valougeorgis, S. Pantazis, K. Jousten, Hybrid modeling of time-dependent rarefied gas expansion, J. Vac. Sci. Technol. 32 (2014) 021602.
[22] K. Jousten, S. Pantazis, J. Buthig, R. Model, M. Wüest, J. Iwicki, A standard to test the dynamics of vacuum gauges in the millisecond range, Vacuum 100 (2014) 14–17.
[23] M. Vargas, S. Naris, D. Valougeorgis, S. Pantazis, K. Jousten, Time-dependent rarefied gas flow of single gases and binary gas mixtures into vacuum, Vacuum 109 (2014) 385–396.
[24] R. Kersevan, J.L. Pons, Introduction to MOLFLOW+: New graphical processing

unit-based Monte Carlo code for simulating molecular flows and for calculating angular coefficients in the compute unified device architecture environment, J. Vac. Sci. Technol. A 27 (2009) 1017–1023.
[25] J. Xu, P.S. Fischbeck, M.J. Small, J.M. VanBriesen, E. Casman, Identifying sets of key nodes for placing sensors in dynamic water distribution networks, J. Water Resources Plan. Management 134 (2008) 378–385.
[26] N. Deo, Graph Theory with Application to Engineering and Computer Science, Prentice-Hall, Englewood Cliffs, NJ, 1974.
[27] A. Ribes, C. Caremoli, Salome platform component model for numerical simulation, Proceedings of the 31st Annual International Computer Software and Applications Conference (2007) 553–564.
[28] G. Pedroche, A.J. Lopez-Revelles, A. Kolsek, M. Dremel, G. Bansal, R. Pearce, J. Sanz, R. Juarez, Nuclear analysis of the ITER torus cryopumps, Nucl. Fusion 59 (2019) 106045.
[29] V. Philipps, J. Ehrenberg, Analysis of outgassing after Joint European torus discharges under beryllium wall conditions, J. Vac. Sci. Technol. A 11 (2) (1993) 437–445.
[30] JET contributors, A. Santucci, M. Incelli, A. Hollingsworth, X. Lefebvre, Z. Kollo, Tritium retention and outgassing from JET first wall materials due to tritiated atmosphere exposure: the tritium soaking facility, 22nd International Conference on Plasma Surface Interactions in Controlled Fusion Devices (2016).
[31] JET EFDA contributors, S. Brezinsek, T. Loarer, et al., Fuel retention studies with the ITER-Like Wall in JET, Nucl. Fusion 53 (2013) 083023.
[32] JET EFDA contributors, V. Philipps, T. Loarer, H.G. Esser, S. Vartanian, U. Kruezi, S. Brezinsek, G. Matthews, Dynamic fuel retention and release under ITER like wall conditions in JET, J. Nucl. Mater. 438 (2013) 1067–1071.